MOLECULAR IMAGING AND BIOLOGY

Published Online: 20 April 2008

Mol Imaging Biol (2008) 10:154–161
DOI: 10.1007/s11307-008-0140-9

RESEARCH ARTICLE

Assessment of Cerebral Glucose Metabolism in Cat Deafness Model: Strategies for Improving the Voxel-Based Statistical Analysis for Animal PET Studies

Jin Su Kim,[1,4,5,6] Jae Sung Lee,[1,2,4,5] Min-Hyun Park,[3] Hyejin Kang,[1] Jong Jin Lee,[1] Hyo-Jeong Lee,[7] Ki Chun Im,[8] Dae Hyuk Moon,[8] Sang-Moo Lim,[6] Seung-Ha Oh,[3] Dong Soo Lee[1,4,5]

[1]*Department of Nuclear Medicine, Seoul National University College of Medicine, 28 Yungun-Dong, Chongno-Gu, Seoul, 110-744, South Korea*
[2]*Department of Biomedical Sciences, Seoul National University College of Medicine, Seoul, South Korea*
[3]*Departments of Otolaryngology—Head and Neck Surgery, Seoul National University College of Medicine, Seoul, South Korea*
[4]*Interdisciplinary Program in Radiation Applied Life Science Major, Seoul National University College of Medicine, Seoul, South Korea*
[5]*Institute of Radiation Medicine, Medical Research Center, Seoul National University College of Medicine, Seoul, South Korea*
[6]*Molecular Imaging Research Center, Korea Institute of Radiological and Medical Sciences, Seoul, South Korea*
[7]*Department of Otolaryngology, Hallym University College of Medicine, Anyang, South Korea*
[8]*Department of Nuclear Medicine, University of Ulsan College of Medicine, Asan Medical Center, Seoul, South Korea*

Abstract

Purpose: The aim of this study was to establish the procedures for 3D voxel-based statistical analysis of 2-deoxy-2-[^{18}F]fluro-D-glucose-positron emission tomography (FDG-PET) images of a cat's brain obtained using a small animal-dedicated PET system and to assess the utility of this approach in investigating the cerebral glucose metabolism in an animal model of cortical deafness.

Procedures: This study compared several different strategies for the spatial processing of PET data acquired twice from eight cats before and after inducing deafness in terms of the comparability of the statistical analysis results to the established pattern of the cerebral glucose metabolic changes in the deaf animals.

Results: The accuracy of the spatial preprocessing procedures and the statistical significance of the comparison were improved by removing the background activities outside the brain regions. The use of the spatial normalization parameters obtained from the mean image of the realigned data set for individual data also helped improve the statistical significance of the paired *t* testing. It was also found that an adjustment of the registration options was also important for increasing the precision of the realignment.

Conclusions: A method for voxel-based analysis of the PET data of a cat's brain was optimized. The results demonstrated the high localization accuracy and specificity of this method, which is expected to be useful for examining the brain PET data of medium-sized animals such as cats.

Key words: Animal PET, Cat, Cerebral glucose metabolism, Voxel-based analysis, Statistical parametric mapping

Correspondence to: Jae Sung Lee; *e-mail:* jaes@snu.ac.kr

Introduction

2Deoxy-2-[^{18}F]fluro-D-glucose (FDG) brain positron emission tomography (PET) provides three-dimensional information on the spatial distribution of glucose metabolism in the brain, with uniform resolution and accuracy over the whole brain. Several investigations on the cerebral glucose metabolism in humans with congenital or acquired profound sensory loss have reported cerebral glucose metabolism patterns in the rest state that differ from those of normal people [1–5]. These findings suggest that neuronal reorganization occurs in sensory-related brain regions due to the absence of sensory input over an extended period of time [6, 7]. This hypothesis has been partly proven by brain activation studies based on functional magnetic resonance imaging (fMRI) or $H_2^{15}O$ PET scans and temporary lesion studies utilizing repetitive transcranial magnetic stimulation (rTMS) [8, 9].

However, little is known about the dynamics of these metabolic changes, as longitudinal and repetitive FDG-PET scans for investigative purposes without proven medical benefit are limited in human subjects due to the hazards of radiation exposure. For the same reason, it is also difficult to compare the cerebral glucose metabolisms of these subjects with those of age-matched normal controls, for example, to examine different patterns of neuronal reorganization during the development. Therefore, it was suggested that autoradiographic assessments of cerebral glucose metabolism be conducted in animal models of cortical deafness [10], and subsequently, a data analysis method for the voxel-wise statistical analysis of 2-[1-^{14}C]-deoxy-D-glucose (2DG) autoradiographic images was developed [11]. However, a large number of animals must be scarified to obtain a sufficiency of sample points at different times after the onset of deafness. Thus, such experiments are demanding in terms of cost and time and potentially increase experimental uncertainties due to inter-animal variability.

Modern PET imaging advances continue to provide more efficient and accurate means for conducting neuronal plasticity research [12–14]. Currently available animal-dedicated PET systems with high resolution and sensitivity allow longitudinal studies to be performed on single animals, with obvious advantages over *ex vivo* studies [15–17].

Voxel-based statistical analysis methods, such as statistical parametric mapping (SPM) and 3D-stereotactic surface projections (3D-SSP), are widely used in imaging studies of the human brain. However, they have not been optimized for the data of animal brains, which has sometimes resulted in erroneous spatial realignment and normalization. The aim of this study is to establish the procedures for the 3D voxel-based statistical analysis of cat brain FDG-PET images obtained using a small animal-dedicated PET system and assess the utility of this approach to investigate the cerebral glucose metabolism in an animal model of cortical deafness. For this purpose, this study compared several different strategies for the spatial processing of PET data acquired twice from eight cats before and after inducing deafness in terms of the correlation between the statistical analysis results and the established pattern of cerebral glucose metabolic changes in deaf animals. We also performed region-of-interest (ROI) analysis for the comparison.

Materials and Methods

Animal Model for Deafness

This animal study was approved by the Institutional Animal Care and Use Committee (IACUC) of Seoul National University. Kanamycin (300 mg/kg) was injected subcutaneously and, 30 minutes later, intravenous ethacrynic acid infusion was started at an infusion rate of 1 mg/min. Infusion was stopped when evoked potential showed no response at 90 dB sound pressure level (SPL). Hearing levels were confirmed 2 weeks later by measuring auditory evoked potentials [18].

Small-Animal PET Scanner

A microPET Focus 120 (F120) scanner (Siemens Medical Solutions, Inc., Knoxville, TN, USA) was used throughout [15]. The detector material was an LSO crystal (Siemens Medical Solutions, Inc., Knoxville, TN, USA), which has a high stopping power, high light output, and a fast decay time. The axial field of view of the scanner was 7.6 cm with a ring diameter of 15 cm (transaxial field of view=10 cm). The sensitivity of the scanner used was 7.0% in the center of its field of view (FOV), for a centered point source. The spatial resolution was 1.18 (radial), 1.13 (tangential), and 1.45 (axial with oversampling) mm full-width at half-maximum (FWHM) at the center, and 2.35 (radial), 1.66 (tangential), and 2.00 mm FWHM (axial with oversampling) at a radial offset of 2 cm [15].

FDG PET Data Acquisition

Eight cats underwent FDG-PET scans before and after inducing deafness. The interval between the operation to induce deafness and second PET scan was 125.3±15.2 days. Before PET scanning, cats were fasted for at least 8 hours. The PET scans were performed in a dark room with an eye bandage to prevent visual stimulation. The background noise level of the scanning room was 65 dB SPL. The cats were anesthetized initially with an intramuscular injection of ketamine and xylazine mixture (100 and 10 mg/kg, respectively) and, subsequently, ketamine was injected intravenously every 30 minutes to maintain anesthesia. After achieving anesthesia, the 40-minute transmission data was acquired using a ^{68}Ge point source with an energy window of 460~560 keV and singles mode. Thirty minutes after the intravenous injection of 1 mCi/kg ^{18}F-FDG, the 30-minute emission data was acquired with an energy window of 350~650 keV and a coincidence window of 6 ns.

All the PET data was acquired in listmode. The transmission listmode data was histogrammed into a 2D sinogram using SSRB, and the scattered data was corrected using a single scatter simulation algorithm. The emission listmode data was rebinned into a 3D sinogram and reconstructed using a 3DRP reconstruction algorithm (*matrix size* = 128 × 128 × 95). The attenuation and scatter corrections for the emission PET data were performed. The image pixel sizes were 0.86 mm transaxially and 0.79 mm axially. In the microPET image, patterns of brain gyral convolution and intensity contrast between gray and white matters are relatively well represented.

Voxel-Wise Statistical Analysis

SPM5 software [19, 20] was used for image analysis. Generally, the PET images are spatially normalized onto a study-specific cat brain template and are smoothed with a Gaussian kernel, and voxel-based paired *t* tests are then performed.

Six different strategies for spatial preprocessing (image realignment and spatial normalization) were compared to determine the optimal strategy for the cat brain PET data analysis. Figure 1 gives a description of these

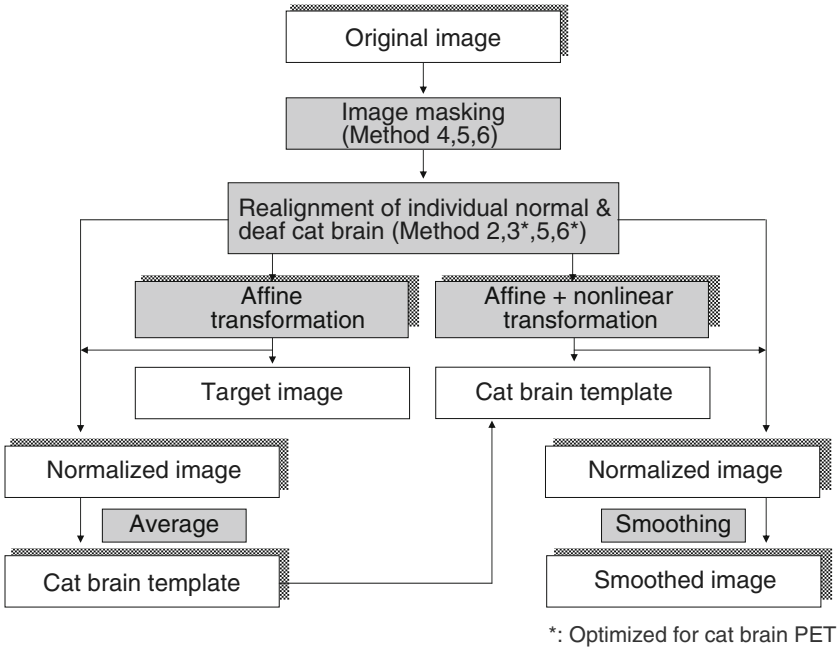

Fig. 1. Schematic diagram of the six different methodologies for voxel-based analysis of cat brain PET data.

methods. In methods 1~3, the original whole brain images were used for spatial preprocessing, whereas in methods 4~6, only the brain and adjacent regions in each data set were masked manually when applying these procedures. The smallest 3D rectangular box required to contain a brain was determined manually.

In methods 1 and 4, each PET data set was normalized directly onto the target brain or study-specific template without realignment between images from the same animals. On the other hand, in methods 2~3 and 5~6, the normal and deaf PET data of the same cat were realigned to each other. The mean images of the realigned data were spatially normalized onto the template, and the normalization parameters were reapplied to the individual PET data.

The distance between the sampling points on the reference image and the kernel size of the Gaussian filter applied to the images before estimating the realignment parameters were adjusted from 4.0 and 5 mm (defaults for human data: methods 2 and 5) to 0.5 and 2 mm (methods 3 and 6), respectively.

To create a study-specific cat brain template, a PET image having good quality and symmetry was selected as a target image from the data set. The target image was then smoothed using an isotropic Gaussian kernel with an FWHM of 2 mm to facilitate the fitting of individual images to the target image. Individual images (methods 1 and 4) or mean images of the realigned data (methods 2~3 and 5~6) were spatially normalized onto the target image using only the affine transformation. The normalized images were then averaged and smoothed with a 2-mm Gaussian kernel to create the final template.

PET images were spatially normalized onto the template using sequential affine and nonlinear transformations. The smoothing kernel size of the source image was modified from 8 to 2 mm. The voxel size of the spatially normalized images was set to 0.3 mm×0.3 mm×0.3 mm. To assess the correctness of the realignment and spatial normalization procedures, we used image fusion software, FIRE [21].

Spatially normalized images were smoothed by convolution using an isotropic Gaussian kernel with a 3-mm FWHM. A kernel size of 3 mm was used, as the resolution of the microPET images was approximately 1.5 mm, and a kernel size of two to three times the spatial resolution was recommended for data smoothing before voxel-wise statistical analysis using the SPM software package. The pixel values of the smoothed PET images were normalized with respect to the global mean of the image intensity. Voxel-wise paired *t* test was then performed to identify hypo- or hypermetabolic areas in the brains after inducing the deafness.

Comparisons with ROI Analysis

The findings of the voxel-based analyses using the six different strategies for spatial preprocessing were compared with the conventionally used ROI-based method. To facilitate ROI drawing, the images were reoriented so that the brain appears to be symmetric on the coronal plane. A neuroscientist, who was blinded to the SPM results, drew the ROIs on the frontal, parietal, and occipital lobes, precentral, postcentral, superior temporal (STG), middle temporal (MTG), inferior temporal (ITG), and cingulate gyri, thalamus, caudate head, inferior colliculus (IC), and superior colliculus (SC) in both hemispheres using MRIcron software referring a cat brain atlas [22]. Figure 2 shows the ROIs drawn on a cat brain PET data. The regional mean pixel values in each ROI were normalized to the mean count of the whole brain, and a paired *t* test between the normal and deaf data were performed in a similar manner to the voxel-wise analysis.

Results

Figure 3a shows the realigned images (left: normal, right: deaf) of a cat brain without brain masking procedure, where the inaccurate realignment of the images was observed. Figure 3b shows the results of the realignment of the same data set after applying the brain masking, highlighting the improved accuracy of the image realignment by preprocessing the raw image data.

Figure 4 shows the transaxial, coronal, sagittal slice of the study-specific cat brain template composed of the all 16 PET data sets and generated using method 6, which was found to be the most optimal method. The template has the average features in shape and intensity, and all the cortical areas and subcortical regions, such as the thalamus, caudate, SC, and IC, are well identified.

Figure 5 shows the results of the voxel-wise statistical analyses using six different strategies for spatial preprocess-

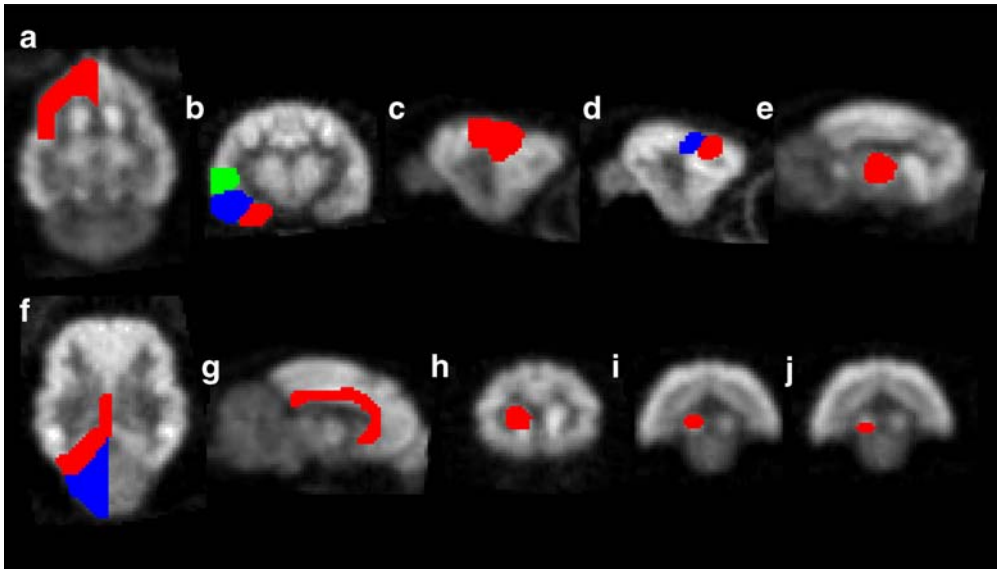

Fig. 2. ROIs drawn on a cat brain PET data. **a** frontal, **b** superior, middle and inferior temporal, **c** parietal, **d** precentral and postcentral, **e** thalamu, **f** occipital and cerebellum, **g** cingulate, **h** caudate, **i** superior colliculus, and **j** inferior colliculus. The ROIs were drawn on the opposite hemisphere.

ing (A~F correspond to methods 1~6, respectively). A *P* value of 0.001 (uncorrected) and cluster size (*k*) of 50 were the thresholds for statistical significance.

Generally, brain masking helped improve the statistical significance of the SPM analysis. Methods 1~2 (no realignment and realignment with the default parameters, respectively, but without brain masking) showed no significant decrease or increase in the cerebral glucose metabolism after inducing deafness under this threshold level (Fig. 5 A~B). Without masking, only method 3 (realignment between the images from the same cat with the adjusted parameters) showed significant findings (decreased glucose metabolism in the STG in the left hemisphere).

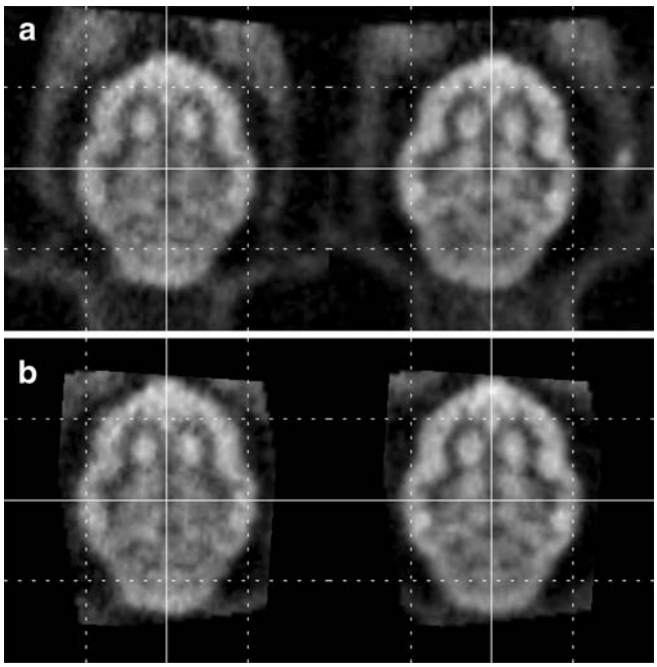

Fig. 3. Realigned images of a cat brain. **a** The default realign parameter (sampling distance=4 mm, smoothing kernel=5 mm) was used without brain masking. **b** The optimized realign parameter (sampling distance=0.5 mm, smoothing kernel=2 mm) was used with brain masking.

Method 4 (brain masking but no realignment) significantly improved the power of the statistical analysis (Fig. 5d). On the other hand, an increase in glucose metabolism in the precentral (border line between precentral and frontal lobe) and parietal regions was observed when method 4 was applied, which did not match with the results of ROI analysis (Table 1).

Figure 5e and f shows that the performance of the statistical analysis was improved significantly by applying the realignment between the normal and deaf PET data from the same animal. The regions of the significant decrease after inducing deafness are well localized in the auditory-related areas (i.e., temporal cortex), and the false finding of an increased metabolism shown with method 4 did not appear. A larger significant region was obtained when the realignment parameter was adjusted for the size of a cat's brain (Fig. 5f: method 6). Only method 6 resulted in clusters with significant metabolic change when a more conservative statistical threshold [corrected *P* based on False Discovery Rate (FDR) <0.05] was applied (Table 1).

Table 1 shows a comparison of the results of the voxel-based statistical analysis (SPM) using method 6 with those obtained by ROI analysis. In SPM analysis, the cerebral glucose metabolism decreased significantly after the loss of hearing in the parietal lobes, postcentral gyri, STG, MTG,

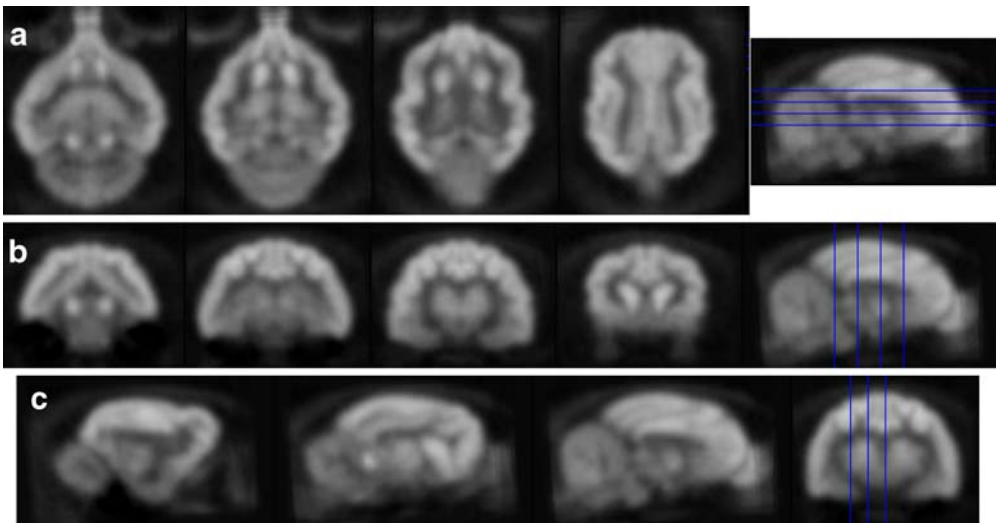

Fig. 4. **a** Transverse, **b** coronal, and **c** sagittal slices of the study-specific cat brain template.

ITG, and IC at both hemisphere and left SC (FDR corrected $P<0.05$, $k>50$). When applying a slightly looser threshold level (uncorrected $P<0.005$, $k>50$), the right SC also showed decreased metabolism in the deafness condition.

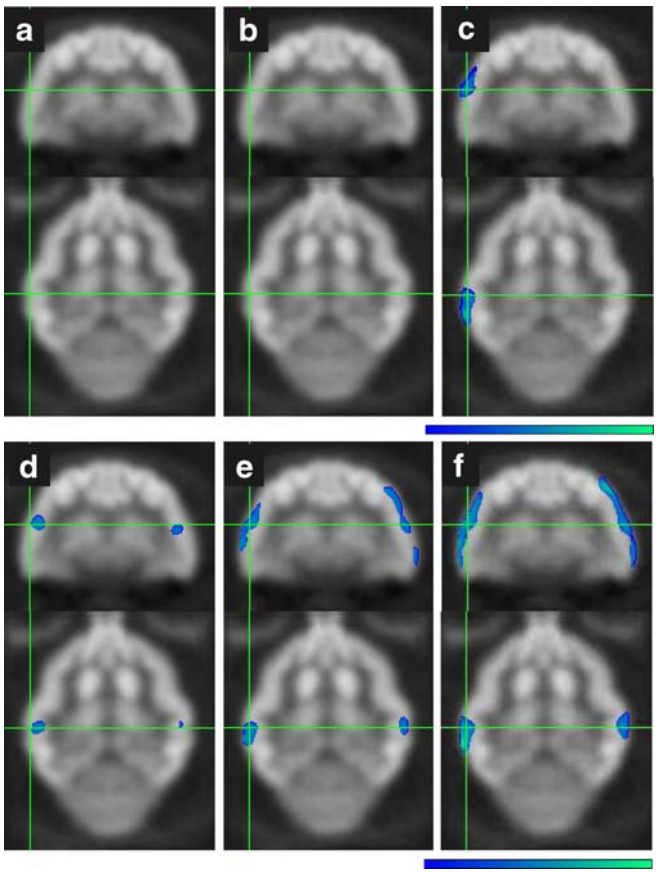

Fig. 5. The brain regions showing decreased regional FDG uptake after inducing deafness. **a**~**f** are corresponding to methods 1~6, respectively.

The brain regions with the higher glucose metabolism in deafness condition included the frontal and occipital lobes at both hemispheres and the left cingulate and occipito-temporal regions (uncorrected $P<0.005$, $k>50$). These findings correspond well with those obtained by ROI analysis (uncorrected $P<0.05$) with the only exceptions being left frontal and right occipital regions.

Local maximum T values (fourth column in the Table 1) derived using the SPM analysis were in general higher than those obtained using the ROI analysis (tenth column). On the contrary, average T values (6th column) obtained by applying the same ROI defined on the target brain onto the SPM T-map generated with the same height threshold ($P<0.05$) as used in the ROI analysis showed smaller differences (range −2.02~1.75) from the ROI-based T values than the maximum T values (range 1.1~19.1).

Discussion

PET is increasingly being used for neuroimaging studies in different animal models primarily because these studies can fill the gap between experimental and clinical studies. The cat is an ideal animal for translational neuroimaging studies because of the amount of information available on its neuronal system. However, a few PET studies have been conducted on the cat brain to date because it is too small to obtain PET images with sufficient anatomical detail using conventional clinical PET scanners with a spatial resolution of 4~6 mm [23–25]. However, recently, PET systems with much higher resolutions have been developed for small animal imaging [15–17, 26, 27]. Nevertheless, these systems have been mainly used for rodent studies, and to date, relatively little work has been performed on the cat brain. The microPET F120 used in the present study is the animal PET scanners widely used for the rodent imaging. These units have a ring diameter of 15 cm and an axial FOV of

Table 1. Comparison of the findings by voxel-based analysis with those from the conventionally used ROI-based methods

L/R	Brain region	SPM analysis					ROI analysis				
		Local maxima			Average[a]		Mean±SD		*T* value	*P* value	
		Cluster size	*T* value	*P* value (FDR)	*T* value		Control	Deaf			
Left	Frontal	(838)	(3.49)	NS	(2.64)	↑	1.19±0.08	1.21±0.08	NS	NS	
	Precentral	–	NS	NS	–		1.53±0.36	1.43±0.07	NS	NS	
	Postcentral	9,404	9.75	<0.05	3.66	↓	1.49±0.14	1.35±0.13	4.01	<0.000	↓
	Parietal	9,404	6.66	<0.05	3.29	↓	1.39±0.12	1.34±0.09	3.38	<0.05	↓
	Occipital	(445)	(5.20)	NS	(2.74)	↑	1.00±0.09	1.06±0.09	3.07	<0.05	↑
	Cerebellum	–	NS	NS	–		0.93±0.12	0.91±0.08	NS	NS	
	STG[b]	9,404	5.23	<0.05	3.57	↓	1.15±0.06	1.06±0.10	1.91	<0.05	↓
	MTG[c]	9,404	11.84	<0.05	4.46	↓	1.01±0.06	0.93±0.12	2.77	<0.05	↓
	ITG[d,e]	9,404	6.73	<0.05	3.10	↓	0.86±0.10	0.79±0.14	3.14	<0.05	↓
	Cingulate	(30,522)	(7.29)	NS	(3.81)	↑	1.20±0.08	1.28±0.04	2.06	<0.05	↑
	Thalamus	–	NS	NS	–		1.11±0.12	1.14±0.14	NS	NS	
	Caudate	–	NS	NS	–		1.32±0.08	1.36±0.07	NS	NS	
	SC[f]	909	4.68	<0.05	4.26	↓	1.37±0.16	1.12±0.12	4.49	<0.000	↓
	IC[g]	909	5.66	<0.05	3.69	↓	1.36±0.17	1.08±0.16	5.71	<0.000	↓
Right	Frontal	(333)	(4.13)	NS	(2.17)	↑	1.15±0.11	1.22±0.05	0.77	<0.05	↑
	Precentral	–	NS	NS	–		1.47±0.36	1.35±0.10	NS	NS	
	Postcentral	9,707	5.72	<0.05	4.70	↓	1.49±0.11	1.30±0.14	5.13	<0.000	↓
	Parietal	9,707	9.28	<0.05	4.44	↓	1.37±0.10	1.24±0.08	3.42	<0.05	↓
	Occipital	(1,026)	(4.75)	NS	(2.77)	↑	1.02±0.08	1.03±0.09	NS	NS	
	Cerebellum	–	NS	NS	–		0.91±0.12	0.92±0.10	NS	NS	
	STG[b]	9,707	6.08	<0.05	3.54	↓	1.11±0.04	1.03±0.08	2.75	<0.05	↓
	MTG[c]	9,707	9.05	<0.05	4.44	↓	0.99±0.07	0.94±0.05	4.19	<0.000	↓
	ITG[d,e]	9,707	5.43	<0.05	4.72	↓	0.82±0.12	0.76±0.13	2.97	<0.05	↓
	Cingulate	76	21.38	<0.05	3.76	↑	1.20±0.08	1.26±0.07	2.21	<0.05	↑
	Thalamus	–	NS	NS	–		1.14±0.10	1.14±0.14	NS	NS	
	Caudate	–	NS	NS	–		1.30±0.11	1.36±0.14	NS	NS	
	SC[f]	(2,378)	(4.93)	NS	3.45	↓	1.35± 0.20	1.12±0.21	3.20	<0.05	↓
	IC[g]	67	4.93	<0.05	3.06	↓	1.28±0.21	1.01±0.20	3.91	<0.000	↓

Cluster size and *T* value was at the condition of the lower *P* value (uncorrected $P<0.005$) when the parentheses were used. This is not significant at the *P* value (FDR corrected $P<0.05$).
NS Not significant
↑ Cerebral glucose metabolism of the deaf cats was higher than that of the controls
↓ Cerebral glucose metabolism of the deaf cats was lower than that of the controls
[a]Average *T* value obtained by applying the ROI onto the SPM *T*-map that was generated with the same height threshold (uncorrected $P<0.05$) as in the ROI analysis.
[b]Superior temporal gyrus
[c]Middle temporal gyrus
[d]Inferior temporal gyrus
[e]Cerebral glucose metabolism at the ITG of deaf cats was lower than those of the controls. However, their site between ITG and MTG was marginal.
[f]Superior colliculus
[g]Inferior colliculus

7.6 cm. Designs have been optimized for the whole-body imaging of rodents (mainly the rat and mouse). However, it was reported that the F120 scanner can be employed to scan the cat brain in excellent anatomical detail, and we also confirmed that transaxial and axial FOVs of the F120 scanner enable PET imaging of the cat brain [15].

For voxel-based analysis of group data from multiple subjects, the most important prerequisite image processing steps would be the image realignment (co-registration of the images using rigid-body transformation) and spatial normalization of the brain (anatomical standardization to have the same size, shape, and local variations). In the SPM software, the mean squared intensity difference between the images is minimized for these image realignment and spatial normalization procedures. Although these algorithms were developed for human brain images, there is no reason that the underlying principle should be different between the species. However, statistical analysis of the cat brain PET data using these spatial preprocessing procedures resulted in a low level of statistical significance in the comparison previously established showing significant results when the extracerebral activities were not treated appropriately (methods 1~3). This may have been because optimization parameters for these spatial preprocessing procedures, e.g., the termination criterion used for optimization are optimized for the human brain and because regional distributions of FDG uptake in the brain and background regions differ in humans and cats. It is known that the ketamine and xylazine anesthetic mixture used in this study decreases global cerebral glucose metabolism, although relative regional distributions are only

minimally affected [28]. We experienced a similar error in the spatial normalization of the autoradiographic data of rat brain in a previous study and overcame this problem by removing the background activity outside the brain before spatial normalization [11]. The accuracy of spatial preprocessing procedures and the statistical significance of the comparison were increased considerably in this study by removing the background activities outside the brain regions (methods 4~6 vs methods 1~3).

For the masking procedure, we initially used the more sophisticated segmentation method to create the brain-specific mask. However, we could not find differences in the results of the spatial preprocessing and statistical analysis on the cat brain FDG-PET data masked with the brain-specific and simple rectangular masks. There are several possible reasons explaining why the simple rectangular masks were enough for the cat brain PET data. The contrast between the cerebral cortex and neighboring structures, such as the cerebrospinal fluid and skull, is clear as shown in Figs. 2 and 3, although there are large extracerebral regions with measurable FDG uptake (mainly soft tissue uptake) around the cat brain. The relative uptake in brain was also enhanced by the attenuation corrections for these images. In addition, no high radioactivity uptake in Harderian glands, which often exhibit high activity in rodents, was not observed in the cat brain PET images (Fig. 4a).

These results also suggest that the use of spatial normalization parameters obtained from the mean image of the realigned data set for an individual data set can improve the statistical significance of paired *t* testing (methods 5 and 6 vs method 4). Because the difference in intensity between the template and source images was minimized to determine the optimal spatial normalization parameters, there might be a trend where the volume of the regions with a wide deviation of intensities (higher or lower) from the template is intentionally contracted by the nonlinear deformation during spatial normalization. Therefore, an estimation of spatial normalization parameters from the mean image, which has a more similar intensity as the study-specific template (overall mean of all the normal and deaf data sets) than the individual deaf or normal data, and the application of these common parameters to the individual data would be a reasonable choice.

It was also found that an adjustment of the registration options to increase the level of precision of the realignment is also important for improving the statistical significance in the analysis of the cat brain data (method 6 vs method 5). The default sampling distance between the points in the reference image and the smoothing kernel size (4 and 5 mm, respectively) that might be optimized for a human data set would be too coarse to obtain accurate registration results on the microPET data set with a finer spatial resolution (<1.5 mm) and voxel size (~0.8 mm) than the human PET data. In contrast, there was no increase in statistical significance after adjusting the other estimation options, such as the degree of B-spline interpolation for data sampling.

In this study, it was found that the cerebral glucose metabolism was significantly lower in the parietal lobe, postcentral gyrus, STG, MTG, ITG, SC, and IC. The results of the voxel-based analysis matched well with those obtained using a conventional ROI method, demonstrating the feasibility of this method as an alternative image analysis tool for the PET data of a cat's brain. The decreased glucose metabolism in the primary auditory and association area at STG and MTG, and the important mediation areas in the auditory pathway, such as IC, is also a relevant finding associated with the lack of auditory input in the deafness model. Our results also showed that clusters with significant hypometabolism around the auditory cortex reached the parietal lobes and postcentral gyri, indicating a relation or dependence between these areas. Loss of auditory function due to deafness might affect the neuronal activities of other intact sensory or association areas, such as the somatosensory and parietal regions. Abnormal cortical development after the onset of deafness is also a possible reason for this hypometabolism. To verify the neuronal basis of hypometabolism in these areas, further tests on the visual–spatial representations and somatosensory functions of deaf animals are required. As the extents of interregional metabolic correlations between the primary auditory cortex and other regions subside with age or deafness duration in humans [29], longitudinal observations on these animals are necessary to better understand the developmental sequence of metabolic connectivity from the auditory cortex in human deafness.

A comparison of voxel-based analysis findings with those obtained using conventional ROI-based methods (Table 1) showed that *T* values obtained by ROI analysis in native space are generally less than 50% of maximum *T* values derived using the optimized SPM method, except for the superior and inferior colliculi. It is difficult to define appropriate positions, sizes, or shapes of ROIs on particular regions during ROI analysis if the operator is blinded to the expected results. Moreover, regional activities obtained using ROI analyses are the averages of active and background signals, and are thus diminished when ROIs are too large. On the contrary, the maximum SPM *T* values are based on a single voxel. Accurate ROI positioning becomes more problematic for smaller ROIs, and therefore, the findings of voxel-based analyses are generally more statistically significant than those of ROI analysis [30]. Moreover, similar levels of significance for small but distinct structures, such as, the superior and inferior colliculi, obtained using these two methods provide a clue concerning the size and positional dependencies of ROI analysis. The smaller differences of average SPM *T*-values from the ROI-based ones than those of maximum SPM *T*-values also indicate that the lower significances in ROI analysis is attributed to the signal averaging. The reason of a slight tendency to higher average SPM *T* values than ROI-based ones in Table 1 would be mainly because the average SPM *T*-values were estimated using only the voxels with smaller *P* values than the height threshold.

Conclusion

In this study, we developed and optimized the method for the voxel-based analysis of cat brain PET data. The results obtained demonstrated the high localization accuracy and specificity of the developed method and were found to be useful for examining cerebral glucose metabolism in a cat cortical deafness model.

Acknowledgements. This work was supported by grants from the Seoul National University Hospital (04-2007-037) and the Basic Research Program of the Korea Science and Engineering Foundation (R01-2006-000-10296-0), Brain Research Center of the 21st Century Frontier Research Program (M103KV010017-07K2201-01710), and Basic Atomic Energy Research Institute Program (M20508050002-05B0805-00210, 2007-01022) funded by the Ministry of Science and Technology. The authors appreciate the experimental support of Kim Seung Jeong, Lee Ho Sun, and Park Soo-Ah and software application support of David L. Bailey (Siemens Molecular Imaging).

References

1. Ito J, Sakakibara J, Iwasaki Y, Yonekura Y (1993) Positron emission tomography of auditory sensation in deaf patients and patients with cochlear implants. Ann Otol Rhinol Laryngol 102:797–801
2. Catalan-Ahumada M, Deggouj N, De Volder A et al (1993) High metabolic activity demonstrated by positron emission tomography in human auditory cortex in case of deafness of early onset. Brain Res 623:287–292
3. Deggouj N, Devolder A, Catalan M et al (1995) Positron emission tomography in deaf patients at rest. Adv Otorhinolaryngol 50:31–37
4. Lee DS, Lee JS, Oh SH et al (2001) Cross-modal plasticity and cochlear implants. Nature 409:149–150
5. Lee JS, Lee DS, Oh SH et al (2003) PET evidence of neuroplasticity in adult auditory cortex of postlingual deafness. J Nucl Med 44:1435–1439
6. Bavelier D, Neville HJ (2002) Cross-modal plasticity: where and how? Nat Rev Neurosci 3:443–452
7. Cordes M, Wszolek ZK (2003) Deafness and cerebral plasticity. J Nucl Med 44:1440–1442
8. Cohen LG, Celnik P, Pascual-Leone A et al (1997) Functional relevance of cross-modal plasticity in blind humans. Nature 389:180–183
9. Nishimura H, Hashikawa K, Doi K et al (1999) Sign language 'heard' in the auditory cortex. Nature 397:116
10. Ahn SH, Oh SH, Lee JS et al (2004) Changes of 2-deoxyglucose uptake in the rat auditory pathway after bilateral ablation of the cochlea. Hear Res 196:33–38
11. Lee JS, Ahn SH, Lee DS et al (2005) Voxel-based statistical analysis of cerebral glucose metabolism in the rat cortical deafness model by 3D reconstruction of brain from autoradiographic images. Eur J Nucl Med Mol Imaging 32:696–701
12. Kornblum HI, Araujo DM, Annala AJ et al (2000) In vivo imaging of neuronal activation and plasticity in the rat brain by high resolution positron emission tomography (microPET). Nat Biotechnol 18:655–660
13. Moore TH, Osteen TL, Chatziioannou TF, Hovda DA, Cherry TR (2000) Quantitative assessment of longitudinal metabolic changes in vivo after traumatic brain injury in the adult rat using FDG-microPET. J Cereb Blood Flow Metab 20:1492–1501
14. Mir HM, Tatsukawa KJ, Carmichael ST, Chesselet MF, Kornblum HI (2004) Metabolic correlates of lesion-specific plasticity: an in vivo imaging study. Brain Res 1002:28–34
15. Kim JS, Lee JS, Im KC et al (2007) Performance measurement of the microPET Focus 120 scanner. J Nucl Med 48:1527–1535
16. Tai YC, Ruangma A, Rowland D et al (2005) Performance evaluation of the microPET focus: a third-generation microPET scanner dedicated to animal imaging. J Nucl Med 46:455–463
17. Schafers KP, Reader AJ, Kriens M et al (2005) Performance evaluation of the 32-module quadHIDAC small-animal PET scanner. J Nucl Med 46:996–1004
18. Xu SA, Shepherd RK, Chen Y, Clark GM (1993) Profound hearing loss in the cat following the single co-administration of kanamycin and ethacrynic acid. Hear Res 70:205–215
19. Friston KJ, Ashburner J, Frith CD et al (1995) Spatial registration and normalization of images. Human Brain Mapping 3:165–189
20. Ashburner J, Friston KJ (1999) Nonlinear spatial normalization using basis functions. Hum Brain Mapp 7:254–266
21. Lee JS, Park KS, Lee DS et al (2005) Development and applications of a software for Functional Image Registration (FIRE). Comput Methods Programs Biomed 78:157–164
22. Reinoso-Suarez F (1961) Topographisher Hirnatlas der Katze. Merck, Darmstadt, Germany
23. Heiss WD, Graf R, Lottgen J et al (1997) Repeat positron emission tomographic studies in transient middle cerebral artery occlusion in cats: residual perfusion and efficacy of postischemic reperfusion. J Cereb Blood Flow Metab 17:388–400
24. Nariai T, Shimada Y, Ishiwata K et al (2003) PET imaging of adenosine A_1 receptors with ^{11}C-MPDX as an indicator of severe cerebral ischemic insult. J Nucl Med 44:1839–1844
25. Ginovart N, Wilson AA, Houle S, Kapur S (2004) Amphetamine pretreatment induces a change in both D2-Receptor density and apparent affinity: a [^{11}C]raclopride positron emission tomography study in cats. Biol Psychiatry 55:1188–1194
26. Surti S, Karp JS, Perkins AE et al (2005) Imaging performance of A-PET: a small animal PET camera. IEEE Trans Med Imaging 24:844–852
27. Rafecas M, Boning G, Pichler BJ et al (2003) Inter-crystal scatter in a dual layer, high resolution LSO-APD positron emission tomograph. Phys Med Biol 48:821–848
28. Matsumura A, Mizokawa S, Tanaka M et al (2003) Assessment of microPET performance in analyzing the rat brain under different types of anesthesia: comparison between quantitative data obtained with microPET and ex vivo autoradiography. Neuroimage 20:2040–2050
29. Kang E, Lee DS, Lee JS et al (2003) Developmental hemispheric asymmetry of interregional metabolic correlation of the auditory cortex in deaf subjects. Neuroimage 19:777–783
30. Nguyen PT, Holschneider DP, Maarek JM et al (2004) Statistical parametric mapping applied to an autoradiographic study of cerebral activation during treadmill walking in rats. Neuroimage 23:252–259